RSK2 inactivation cooperates with AXIN1 inactivation or ß-catenin activation to promote hepatocarcinogenesis

Samantha Schaeffer[1,2]*, Barkha Gupta[1,2]*, Anna-Line Calatayud[1,2]*, Julien Calderaro[3], Stefano Caruso[1,2], Théo Z. Hirsch[1,2], Laura Pelletier[1,2], Jessica Zucman-Rossi[1,2,4], Sandra Rebouissou[1,2].

* These authors contributed equally to this work.

Table of content

JOURNAL
OF HEPATOLOGY

Journal of Hepatology
CTAT methods

Tables for a "Complete, Transparent, Accurate and Timely account" (CTAT) are now mandatory for all revised submissions. The aim is to enhance the reproducibility of methods.

- Only include the parts relevant to your study
- Refer to the CTAT in the main text as 'Supplementary CTAT Table'
- Do not add subheadings
- Add as many rows as needed to include all information
- Only include one item per row

If the CTAT form is not relevant to your study, please outline the reasons why:

1.1 Antibodies

Name	Citation	Supplier	Cat no.	Clone no.
RSK2		Cell signaling	5528	
Glutamine synthetase		BD Biosciences	610517	
phospho-ERK (Thr202/Tyr204)		Cell signaling	4376	
KI67		Cell signaling	12202	
ß-catenin		BD Biosciences	610153	
CK7		Abcam	181598	
RSK2		Santa Cruz Biotechnology	sc-1430	
ERK 1/2		Cell Signaling	9102	
phospho-ERK1/2 (Thr202/Tyr204)		Cell Signaling	9101	
β-actin		Sigma	A5060	

1.2 Cell lines

Name	Citation	Supplier	Cat no.	Passage no.	Authentication test method
Hep3B	Aden et al. Nature (1979) [PMID: 233137]	ATCC - USA			WES
Huh7	Nakabayashi et al Cancer Res (1982) [PMID: 6286115]	ATCC - USA			WES
PLC/PRF5	Alexander et al. S Afr Med J (1976) [PMID: 63998]	ATCC - USA			WES
SNU475	Park et al. Int J Cancer (1995) [PMID: 7543080]	ATCC - USA			WES
HepaRG	Gripon et al. PNAS	Gift from			WES

	(2002) [PMID: 12432097]	Philippe Merle and Fabien Zoulim (Inserm U1052, France)			
HepG2	Aden et al. Nature (1979) [PMID: 233137]	ATCC - USA			WES
Huh6	Doi et al. Gan (1976) [PMID: **57894]**	RIKEN BioResource Center - Japan			WES

1.3 Organisms

Name	Citation	Supplier	Strain	Sex	Age	Overall n number
Rsk2$^{-/y}$ mice	Yang et al. Cell (2004) [PMID: **15109498]**	André Hanauer	C57BL/6J	Male		
Axin1$^{fl/fl}$/AhCre mice	Feng et al. Gastroenterology (2012) [PMID: **22960659]**	Trevor Dale	C57BL/6J	Male		

1.4 Sequence based reagents

Name	Sequence	Supplier
RPS6KA3 TaqMan predesigned assay	Hs00177936_m1	Life Technologies
Ribosomal 18S TaqMan predesigned assay	Hs03928990_g1	Life Technologies
Axin1 TaqMan predesigned assay	Mm01299058_m1	Life Technologies
Rps6ka3 TaqMan predesigned assay	Mm00455829_m1	Life Technologies
RPS6KA3 Forward primer (1)	AGGAGATTAACCCACAAACTGAAGA	Invitrogen
RPS6KA3 Reverse primer (1)	TCCAAAATAAGATACAACTTCCCTTCAG	Invitrogen
RPS6KA3 Forward primer (2)	ACAGTTTATTCCAGTCTATCGTTGAGA	Invitrogen
RPS6KA3 Reverse primer (2)	ACAGTTTATTCCAGTCTATCGTTGAGA	Invitrogen
RPS6KA3 Forward primer (3)	GTGCAGGACCAGATGGAGTT	Invitrogen
RPS6KA3 Reverse primer (3)	TGGATGCTGTCCATAACGAA	Invitrogen

RPS6KA3 Forward primer (4)	TCAATTGTTCAGCAGTTACACAGGA	Invitrogen
RPS6KA3 Reverse primer (4)	AGCAGCATCATAGCCTTGTCT	Invitrogen
RPS6KA3 Forward primer (5)	TGAGAGCGGAAAATGGTCTT	Invitrogen
RPS6KA3 Reverse primer (5)	CAGGGCTGTTGAGGTGATTT	Invitrogen
Rps6ka3 Forward primer	TTGTTGGTTTACTTTCTTTCGGTCTG	Invitrogen
Rps6ka3 Reverse primer	AAGATGATTGCTTTGCTTAGTTTA	Invitrogen
Axin1 Forward primer	CCTCAAGTAGACGGTACAACGAAGGCAGAG	Invitrogen
Axin1 Reverse primer	CTGTGCAGGAGCTCTACTAAGCCTCTACAC	Invitrogen
Cre Forward primer	TGACCGTACACCAAAATTTG	Invitrogen
Cre Reverse primer	ATTGCCCCTGTTTCACTATC	Invitrogen

1.5 Biological samples

Description	Source	Identifier
LICA-FR HCC dataset	PMID: **25822088 ;** PMID: **29101368 ;** PMID: **30531861 ;** PMID: **31862487 ;** PMID: **31206197**	
TCGA HCC dataset	PMID: **28622513**	
KOREAN HCC dataset	PMID: **24798001**	
LIRI-JP HCC dataset	PMID: **27064257**	

1.6 Deposited data

Name of repository	Identifier	Link
European Nucleotide Archive (ENA)	PRJEB59874	https://www.ebi.ac.uk/ena/browser/view/PRJEB59874

1.7 Software

Software name	Manufacturer	Version
GraphPad Prism	GraphPad Software	9
R software	R Foundation for Statistical Computing https://www.R-project.org	3.5.1
ImageLab software	Bio-Rad	5.2.1
Sequencher software	Gene codes corporation	
SDS software	Applied Biosystems	
Fluidigm Real-Time PCR Analysis software	Fluidigm	4.1.3

1.8 Other (e.g. drugs, proteins, vectors etc.)

Sorafenib	#S1040	Selleck Chemicals
Refametinib	#S1089	Selleck Chemicals
Trametinib	#S2673	Selleck Chemicals
PF-04691502	#S2743	Selleck Chemicals
Selumetinib	#S1008	Selleck Chemicals
Mirdametinib	#S1036	Selleck Chemicals
RPS6KA3 open reading frame	#OHS5900-224626707	Dharmacon
Empty vector	#OHS5833	Dharmacon
RPS6KA3 siRNA (1)	#s12279	Life Technologies
RPS6KA3 siRNA (2)	#s12280	Life Technologies
RPS6KA3 siRNA (3)	#s12280	Life Technologies
Block-iT Alexa Fluor Red siRNA	#14750100	Life Technologies

1.9 Please provide the details of the corresponding methods author for the manuscript:

sandra.rebouissou@inserm.fr

2.0 Please confirm for randomised controlled trials all versions of the clinical protocol are included in the submission. These will be published online as supplementary information.

NA

Supplementary material and methods

Human tumor datasets

The overall series of human HCCs includes 1151 samples from four different NGS (whole-exome or whole genome) datasets publicly available and previously described: LICA-FR (n=336) [1–5], TCGA (n=353, available on cBioPortal) [6], KOREAN (n=230, available on cBioPortal) [7] and LIRI-JP (n=232, available on the ICGC data portal) [8]. Non-HCC human tumors are all part of the TCGA project available on cBioPortal and includes 9 542 tumors from 34 different cancer types, excluding HCCs (https://www.cbioportal.org/). Only tumors for which information on somatic mutations and copy-number alterations was available were selected for analysis.

Genomic alterations of *RPS6KA3* and other HCC driver genes

Across the HCC series, we analyzed somatic mutations and CNAs in 21 genes frequently altered in HCC including: *RPS6KA3*, *CTNNB1*, *AXIN1*, *APC*, *TP53*, *TERT* promoter (point mutation and HBV insertions, when available), *ARID1A*, *ARID2*, *KMT2D*, *NFE2L2*, *KEAP1*, *ATM*, *RB1*, *CCND1*, *FGF19*, *TSC1*, *TSC2*, *BAP1*, *ALB*, *APOB* and *CDKN2A*. In non-HCC tumors, we only analyzed *RPS6KA3* genomic alterations.

Gene alteration data were extracted from cBioPortal (TCGA and KOREAN datasets) or from the original publications (LICA-FR) except for the LIRI-JP dataset for which copy number profiles were defined using a previously described in-house pipeline [9]. CNA data for *RPS6KA3* localized on the X chromosome were not available for the HCC KOREAN dataset and gene fusions were not analyzed. In the graphical representations, Fig.1A and 1D, for *RPS6KA3*, when two or more alterations were identified in the same sample, only the most functionally deleterious one was represented. In Fig.1D, amplifications and homozygous deletions were not considered for tumor suppressor genes and oncogenes, respectively.

Germline mutations for *RPS6KA3* were obtained from a cohort of 129 patients with Coffin-Lowry syndrome, previously reported in two studies [10,11].

For each category of sample (HCC tumors, non-HCC tumors and Coffin-Lowry patients) we used MutationMapper [12,13] to map mutations along the RSK2 protein sequence and its domains, and the functional effects (“tolerated” or “deleterious”) of RSK2 missense mutations were predicted by SIFT (Sorting Intolerant From Tolerant) algorithm using Annovar annotation. Mutation load in non-HCC tumors was quantified by whole-exome sequencing from cBioPortal data.

Co-occurrence or mutual exclusivity between pairs of mutated genes in HCC was analyzed using the OncoPrinter tool [12,13] of cBioPortal and significance was assessed using a one-sided Fisher’s exact test. Multiple test correction was applied by calculating FDR adjusted p-values (q-values) and the strength of association or exclusion was evaluated by the odds ratio. A q-value<0.05 was considered significant, and a $\log_2$ odds ratio>1 or <-1 indicates a tendency towards co-occurrence or mutual exclusivity, respectively [12,13].

RPS6KA3 mRNA expression

mRNA expression in human tumors was assessed in a series of 210 HCCs from the LICA-FR cohort by quantitative RT-PCR. Reverse transcription was performed using 500 ng of total RNA and the High-Capacity Transcription Kit (Life Technologies). Gene expression was assessed using a predesigned *RPS6KA3* TaqMan assay (Hs00177936_m1; Life Technologies) on Fluidigm 96 dynamic arrays with the Bio-Mark Real-Time PCR system. The expression level (Ct values) was assessed using the Fluidigm Real-Time PCR Analysis

software (4.1.3). The gene expression data were expressed using the $2^{-\Delta\Delta Ct}$ method relative to ribosomal 18S (R18S Hs03928990_g1; Life Technologies) and the expression level of the corresponding gene in normal liver samples. For liver cancer cell lines experiments (RSK2 overexpression and knockdown) *RPS6KA3* mRNA expression was quantified using the same reverse transcription protocol and predesigned TaqMan assays on the Applied Biosystems® 7900 HT Real-Time PCR System.

RSK2 protein expression in human HCC

RSK2 protein expression was assessed in a series comprising of 165 HCCs from the LICA-FR cohort. Proteins were extracted using Laemmli buffer (50 mM Tris pH =6.8, 2% SDS, 5% glycerol, 2 mM DTT, 2.5 mM EDTA, 2.5 mM EGTA, 1x HALT Phosphatase inhibitor (Perbio 78420), Protease inhibitor cocktail complete MINI EDTA-free (Roche 1836170, 1 tablet/10 mL), 2 mM Na3VO4 and 10 mM NaF), using a Precellys (Bertin) and CK28-R tubes containing 2.8 mm ceramic beads. Extracts were then boiled for 10 min at 100°C, sonicated to reduce viscosity and centrifuged 10 min at 15000 rpm. The supernatant was harvested and stored at -80°C. Protein concentration was determined using the Pierce BCA reducing agent compatible kit, (ref 23252). RSK2 expression was assessed by reverse-phase-protein array using anti-RSK2 antibody (Cell signaling, 5528) as previously described [14].

***RPS6KA3* Sanger sequencing on cDNA**

Reverse transcription was performed using 400 ng of total RNA and the SuperScript Vilo MasterMix (ThermoFischer Scientific). PCR amplification of *RPS6KA3* cDNA was then performed using the Multiplex kit (Qiagen), 5 µM of specifically designed primers (Invitrogen) encompassing mutations identified on the genomic DNA (described in the table below) and 40 ng of cDNA with annealing at 56°C. Purification of RT-PCR products was performed using Exostar kit (GE), sequencing PCR was made with the same specific primers and final purification was performed using BigDye Terminator kit (Applied Biosystems). Sequences were analyzed by Sequencher software (Gene codes corporation).

Forward primer (5'-3')	Reverse primer (5'-3')	Sample analyzed
AGGAGATTAACCCACAAACTGAAGA	TCCAAAATAAGATACAACTTCCCTTCAG	CHC4229T
ACAGTTTATTCCAGTCTATCGTTGAGA	ACAGTTTATTCCAGTCTATCGTTGAGA	CHC4229T
GTGCAGGACCAGATGGAGTT	TGGATGCTGTCCATAACGAA	CHC4229T
TCAATTGTTCAGCAGTTACACAGGA	AGCAGCATCATAGCCTTGTCT	CHC018T
TGAGAGCGGAAAATGGTCTT	CAGGGCTGTTGAGGTGATTT	CHC1999T CHC309T

Survival analysis

In patients treated with liver resection, overall survival was defined as the time from resection of the primary tumor to death, from any cause, within 5 years of follow-up. We excluded patients who underwent noncurative resections or liver transplantations and patients who died within 2 months after surgery. Survival rates were determined using the Kaplan-Meier method and the log-rank test.

Mouse models

Mice were housed in a specific pathogen-free facility and experiments were performed according with French government regulations, with the approval of the “Ministère de l'Enseignement Supérieur et de la Recherche Ethics Committee for animal experimentation” (Authorization no. 2015082610113065.01, Ethics Committee Paris-Nord C2EA 121). All mice used in this study were males on a C57BL/6J background. Mice with constitutive and

ubiquitous inactivation of RSK2 (*Rsk2*$^{-/y}$) were generated by Dr. André Hanauer as previously described [15] and floxed *Axin1* mice (*Axin1*$^{fl/fl}$/AhCre mice, bore a conditional *Axin1* allele in which exon 2 was flanked by two loxP sites) were generated by Pr. Trevor Dale as already described [16]. These two models were generously donated to our laboratory, and then bred at our animal facility, housed at a maximum of five per cage under a 12h dark/light cycle, with free access to water and standard mouse food.

A third murine line was developed by intercrossing the previously described mice (*Rsk2*$^{-/y}$ or *Rsk2*^{wt}, and *Axin1*^{fl}/AhCre or *Axin1*^{wt}/AhCre). The following genotypes were thus generated: *Rsk2*^{wt} *; Axin1*^{wt}/AhCre (wild-type mice), *Rsk2*$^{-/y}$ *; Axin1*^{wt}/AhCre (RSK2 inactivated mice), *Rsk2*^{wt} *; Axin1*$^{fl/fl}$/AhCre (AXIN1 inactivated mice), *Rsk2*$^{-/y}$ *; Axin1*$^{fl/fl}$/AhCre (both RSK2 and AXIN1 inactivated mice). Two additional genotypes with monoallelic inactivation of *Axin1* combined or not with RSK2 inactivation were also generated and used as controls in experiments (*Rsk2*^{wt} *; Axin1*$^{wt/fl}$/AhCre and *Rsk2*$^{-/y}$ *; Axin1*$^{wt/fl}$/AhCre).

For simplicity, throughout the manuscript, *Rsk2* has been used instead of *Rps6ka3* to refer to mouse genotypes.

The purity of the C57BL/6J background of the *Rsk2* and *Axin1* mice used for the generation of the different lines was 99.9% and 94% respectively, based on the analysis of a panel of 384 single nucleotide polymorphisms (SNPs) (analysis performed by Charles River).

Genotyping and analysis of gene knock-out

Mice were genotyped by PCR analysis of tail DNA extracted with the “KAPA Mouse Genotyping Kit” (Kapa Biosystems, KK7302) at 3 weeks of age. Touch-down PCR amplification with annealing temperature from 55°C to 60°C gradually reduced (1°C /every second cycle) was performed using the Multiplex kit (Qiagen) for the detection of *Rps6ka3*, *Axin1* and Cre, with 40 ng of DNA and 5 µM of the following specifically designed primers:

- *Rps6ka3* → forward = 5’-TTGTTGGTTTACTTTCTTTCGGTCTG
  reverse = 5’-AAGATGATTGCTTTGCTTAGTTTA
- *Axin1* → forward = 5’-CCTCAAGTAGACGGTACAACGAAGGCAGAG
  reverse = 5’-CTGTGCAGGAGCTCTACTAAGCCTCTACAC
- Cre → forward = 5’-TGACCGTACACCAAAATTTG
  reverse = 5’-ATTGCCCCTGTTTCACTATC

Rps6ka3 and *Axin1* inactivation were also systematically confirmed by qRT-PCR on non-tumor liver tissues after RNA extraction using Maxwell 16 LEV simply RNA tissue kit (Promega #AS1280) followed by reverse transcription using 500 ng of total RNA and the High-Capacity Transcription Kit (Life Technologies). *Rps6ka3* and *Axin1* expression were quantified on cDNA using TaqMan predesigned assays (Mm01299058_m1 for *Axin1* and Mm00455829_m1 for *Rps6ka3*) on the Applied Biosystems® 7900 HT Real-Time PCR System.

Treatments

AXIN1 was inactivated in *Axin1* floxed AhCre mice, by using a transcriptionally inducible Cre recombinase under the control of the promoter element of the rat *Cyp1A1* gene (referred as AhCre previously described [17]). *Axin1* was disrupted in the liver following induction of the Ah promoter and Cre activity by intraperitoneal injections of ß-naphthoflavone (BNF; at 80 mg/kg dissolved in corn oil) over 4 consecutive days, in 6 weeks old mice. All mice from the double knock-out protocol were injected with BNF. In this system, Cre-mediated recombination is obtained in several epithelia of the gastrointestinal tract including small intestine and liver where it is relatively hepatocyte specific [18]. For chemically induced

mouse models of liver cancer, *Rsk2*$^{-/y}$ or wild-type mice were administered with single intraperitoneal injection of DEN (90 mg/kg), according to three different protocols: 1) at 6 weeks old, followed by continuous oral administration of 0.05% phenobarbital (PB) in the drinking water or 2) at 2 weeks old 3) at 6 weeks old.

Necropsy

Mice were sacrificed by cervical dislocation and autopsy was performed, 9 months and 12 months after AXIN1 inactivation, or after DEN injection followed by PB diet. For juvenile (2 weeks old) mice and adult mice (6 weeks old) treated with DEN alone, necropsy was performed 6 months and 12 months after injection, respectively. Mice and livers were weighted, carefully observed, and tissues and tumor burden were analyzed. Macroscopic nodules were also measured and photographed when possible.

Histology and Immunohistochemistry

A portion of each liver lobe and tumors (when macroscopically visible) was fixed in 10% formalin for 48h, before paraffin embedding and sectioning at 5 µm thickness. The remaining liver tissue was immediately frozen in liquid nitrogen and stored at -80°C for molecular analysis.

Slide preparations and image acquisition were done at the “Histology, cell Imaging and flow Cytometry Center (CHIC)” of the CRC (Cordelier’s Research Center).

HES staining and immunohistochemistry were performed on slides that were deparaffinized in xylene, followed by rehydration in ethanol and rinsed in water.

For HES, sections were stained by passing through Mayers’ hemalum solution, lithium carbonate and 1% eosin staining before being dehydrated by graded alcohol, colored by 0.1% safran staining, and finally passed through alcohol and xylene baths. Slides were reviewed independently by two pathologists to confirm the presence of liver tumors and the architectural abnormalities. The number of nodules in the liver was also noted.

Immunohistochemistry was performed according to standard procedure, after antigen retrieval, using a Dako 48ASL automate with the EnVision + HRP System (Agilent K4001 or K4003) coupled with DAB substrate chromogen system. The following antibodies were used: anti-glutamine synthetase antibody (GS, BD Biosciences 610517, pH6, 1/1000), phospho-ERK (Thr202/Tyr204) antibody (Cell Signaling 4376, pH9, 1/100), KI67 antibody (Cell Signaling 12202, pH6, 1/200), ß-catenin antibody (BD Biosciences 610153, pH9, 1/50), CK7 antibody (Abcam 181598, pH9, 1/8000).

GS was considered positive when more than 90% of tumor cells showed cytoplasmic staining. ß-catenin and phospho-ERK staining were considered positive when more than 5% of tumor cells showed nuclear staining. KI67 index was calculated as the average percentage of KI67-positive tumor nuclei among 500 cells counted in 5 consecutive fields after selecting hotspot area. CK7 staining was used to measure bile ducts diameter (mean of 39 bile ducts analyzed per mice) and to quantify the number of oval cells per portal tract according to the criteria used by other authors ([19,20] and see **Fig. S7**) (mean of 23 portal tracts analyzed per mice) and using the QuPath software [21]. More precisely, oval cells have been defined as small cells with an oval nucleus and little cytoplasm found singly, in cluster or organized in cords. The interlobular bile duct is defined as being a tubular structure with a recognizable lumen. For oval cell counting, all interlobular bile ducts (which also show reactivity with CK7) were sought and excluded from counting (see **Fig. S7**).

For phospho-ERK, protein expression was also quantified using the Histoscore (H-score) ranging from 0 to 300 defined as the percentage of positive cells multiplied by the staining

intensity graded as 0 (negative),1 (weak), 2 (moderate) and 3 (strong).

RNA Sequencing of mouse samples

RNA extraction was performed using the Maxwell 16 LEV simply RNA tissue kit (Promega #AS1280) or the AllPrep DNA/RNA/miRNA Universal Kit (Qiagen #80224) following the manufacturer's instructions. Libraries and sequencing were performed by IntegraGen (Evry, France). Libraries were prepared with the NEBNext® Ultra™ II Directional RNA Library Prep Kit for Illumina protocol according to supplier's recommendations.

Briefly, the key steps of this protocol are successively, purification of PolyA containing mRNA molecules using poly-T oligo attached magnetic beads from 100ng total RNA (with the Magnetic mRNA Isolation Kit from NEB), a fragmentation with divalent cations at elevated temperature to obtain approximately 300bp pieces, synthesis of double stranded cDNA and finally Illumina adapters ligation and cDNA library amplification by PCR for sequencing. Sequencing was then carried out on Paired end 100 bp reads on the Illumina NovaSeq6000 system. Image analysis and base calling were performed using Illumina Real Time Analysis with default parameters.

Full Fastq files were aligned to the mm10 reference mouse genome using TopHat2. We removed reads mapping to multiple locations, and we used HTSeq to obtain the number of reads associated to each gene in the Gencode vM21 database. We used the Bioconductor DESeq2 package to import raw HTSeq counts for each sample into R statistical software and apply variance stabilizing transformation (VST) to the raw count matrix. FPKM scores (number of fragments per kilobase of exon model and millions of mapped reads) were calculated by normalizing the count matrix for the library size and the coding length of each gene. We used the area under the ROC curve (AUC) to identify and remove 676 genes with a significant batch effect (AUC > 0.95 between one sequencing project and others).

The Bioconductor DESeq2 package was used to detect differentially expressed genes between the different mouse genotypes in non-tumor liver.

We used an in-house adaptation of the GSEA method to identify gene sets (from the MSigDB v6 database) overrepresented among up- and down-regulated genes.

For tumor samples, we have analyzed all the nodules for which enough material of good quality that was not too contaminated with non-tumor tissue was available.

Ctnnb1, Braf and *Hras* activating mutations in classical hotspots were identified from RNA sequencing data on IGV (Integrative Genomics Viewer). For *Braf*, as the number of reads was not sufficient to assess the mutational status for three cases (2124_T1, 2088_T1 and 2088_T2) we performed Sanger sequencing of DNA as previously described [22].

Data have been deposited on the European Nucleotide Archive at EMBL-EBI: https://www.ebi.ac.uk/ena/browser/view/PRJEB59874

Mouse-human HCC transcriptomic profile comparison

First, we extracted a gene expression signature capable of classifying human HCCs into 6 transcriptomic groups from G1 to G6 [23] from the open-source R package on Github: https://github.com/cit-bioinfo/MS.liverK. We then selected one-to-one orthologous genes in human and mouse from MGI (http://www.informatics.jax.org), two genes (*Myh4* and *Slc12a1*) were removed as they were not expressed in the mouse samples, yielding a 372-gene expression signature.

For both datasets (mouse and human), variance-stabilized expression values were standardized separately for each gene included in the 372 gene-signature to obtain a mean of 0 and a standard deviation of 1 per gene (z-score values). Next, pairwise correlations

between human and mouse HCC samples were determined on the z-score transformed values using Pearson correlation. Hierarchical clustering of the obtained correlation coefficients was done using correlation distance and average linkage method with the Clustvis tool [24].
To test for statistical significance of association between transcriptomic profiles of mouse and human HCCs, in each of the 6 transcriptomic groups we calculated the proportion of human HCCs with an expression profile positively (Pearson's r>0) and significantly (P<0.05) correlated with each mouse HCC and we tested for a statistical enrichment using a Fisher's exact test.

RSK2 overexpression and knockdown

Hep3B cell line was purchased from ATCC and transduced using lentiviral particles from Dharmacon either with the *RPS6KA3* open reading frame (#OHS5900-224626707) or with the empty vector (#OHS5833). 30 000 cells per well were seeded in duplicate in 24-well plate. After 24h at an average confluence of 50%, cells were transduced with lentiviral particles at MOI ranging from 1.25 to 20 in serum-free and antibiotics-free medium. After 6 hours, complete medium was added on top, and complete media was changed after 24h of incubation. Once the cells were sub-confluent, they were selected using 2.5µg/mL of blasticidin previously determined by antibiotics range test. After selection, only MOI 10 and 20 were used for the following experiments.
For RSK2 knockdown experiments, 6 liver cancer cell lines (Huh7, PLC/PRF5, SNU475, HepaRG, HepG2 and Huh6) previously described [14] were transfected with 2 nM of short interfering RNA (siRNA) using the Lipofectamine RNAiMAX reagent (Invitrogen) in six-well plates, according to the manufacturer's protocol. Three different siRNA duplexes targeting *RPS6KA3* (encoding RSK2) (s12279, s12280 and s12280, Life Technologies) were tested. Block-iT Alexa Fluor Red Fluorescent Oligo siRNA (Life Technologies) was used as a double-stranded RNA negative control. The effect of gene knockdown was verified at the mRNA level by qRT-PCR and at the protein level by immunoblotting.

Protein extraction and Western Blot

Total proteins were extracted from Hep3B, Huh7, PLC/PRF5, SNU475, HepaRG, HepG2 and Huh6 cells using 1X RIPA lysis buffer (#20188, Millipore) supplemented with 1X protease, phosphatase inhibitors cocktail (#78440, ThermoFischer). Proteins were separated on 4-20% gels (#5671094, BioRad), transferred to nitrocellulose membrane (1704159, BioRad), and probed with the following antibodies and dilutions: RSK2 (sc-1430, Santa Cruz Biotechnology; 1:2000 dilution), 1/1000 for anti-ERK 1/2 (#9102, Cell Signaling) and anti-phospho-ERK1/2 (Thr202/Tyr204) (#9101, Cell Signaling). Red ponceau or polyclonal rabbit antibody to β-actin (A5060, Sigma; 1:3000 dilution) staining was used as a loading control. Quantification of protein expression was performed using ImageLab 5.2.1 software.

Cell viability assay and drug testing

Parental Hep3B cells transduced or not with the empty vector and Hep3B cells stably overexpressing RSK2 were seeded in 96-well plates at 3000 cells per well. Growth kinetics analysis was performed at the following time points: 24h, 48h, 76h and 120h in triplicate. Drug testing was performed as previously described [14] using the HP D300 digital dispenser (Tecan) with 5 concentrations (in duplicate) of the following compounds (10-fold dilution from 0.001 to 10 µM in duplicates) for 72 hours: Sorafenib (#S1040), Refametinib (#S1089), Trametinib (#S2673) and PF-04691502 (#S2743) purchased from Selleck Chemicals. Cell

viability was assessed by incubating cells with MTS solution (CellTiter 96® AQueous One Solution Cell Proliferation Assay, Promega) diluted 1:6 in fresh culture medium for 2 hours. Absorbance at 490nm was then recorded using a FLUOstar Omega microplate reader (BMG Labtech). Cell viability curves and curve fitting of dose-response data were performed using GraphPad Prism 9 software (GraphPad Software, Inc., La Jolla, CA). For growth kinetics, each value was normalized on day 0. Two parameters reflecting drug sensitivity were derived from dose-response curves: 1) the GI50 corresponding to the concentration of drug that inhibits 50% of cell viability and 2) the AUC corresponding to the area under the dose-response curve that provides an overall measure of cumulative response.
For RSK2 knockdown experiments, cell viability was assessed by a MTT assay measuring absorbance at 540 nm. Selumetinib (#S1008) and mirdametinib (#S1036) were purchased from Selleck Chemicals.

Supplementary Figures

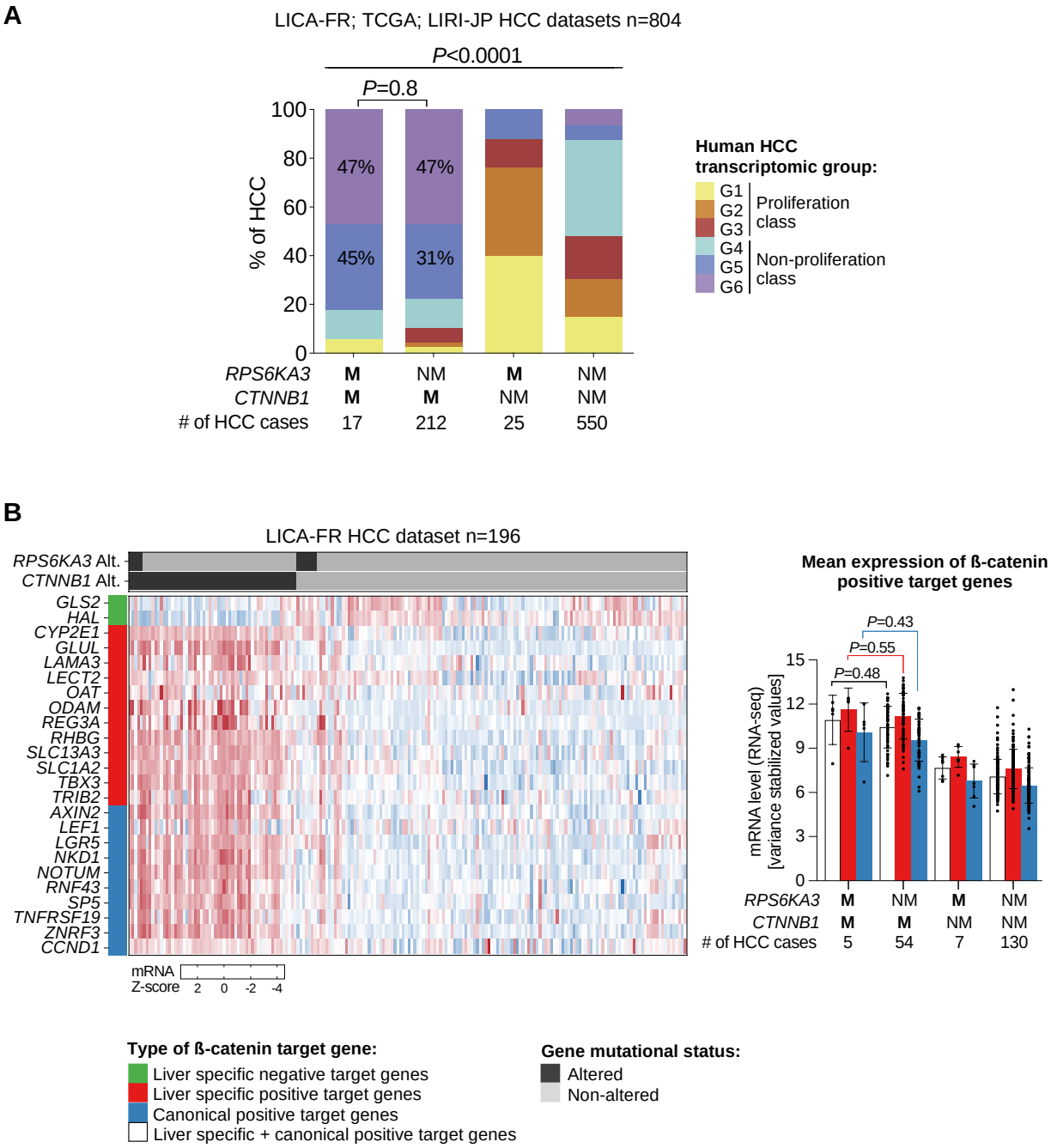

Fig. S1. Analysis of the impact of RSK2 inactivation in ß-catenin mutated human HCCs on the transcriptomic classification and the expression of ß-catenin target genes. (A) Repartition of the different transcriptomic subgroups from the Boyault's classification [23] according to the mutational status of *RPS6KA3*/RSK2 and *CTNNB1* showing no difference between HCCs mutated for both *RPS6KA3* and *CTNNB1* compared to HCC mutated for *CTNNB1* alone (Chi-square test). (B) Left panel: Heatmap showing transcriptional expression of ß-catenin target genes in each HCC sample according to *RPS6KA3* and *CTNNB1* mutational status. Right panel: histograms showing no difference in the mean expression level of positive ß-catenin target genes between HCCs co-mutated for *RPS6KA3* and *CTNNB1* and HCCs mutated for *CTNNB1* alone (two tailed t-test).

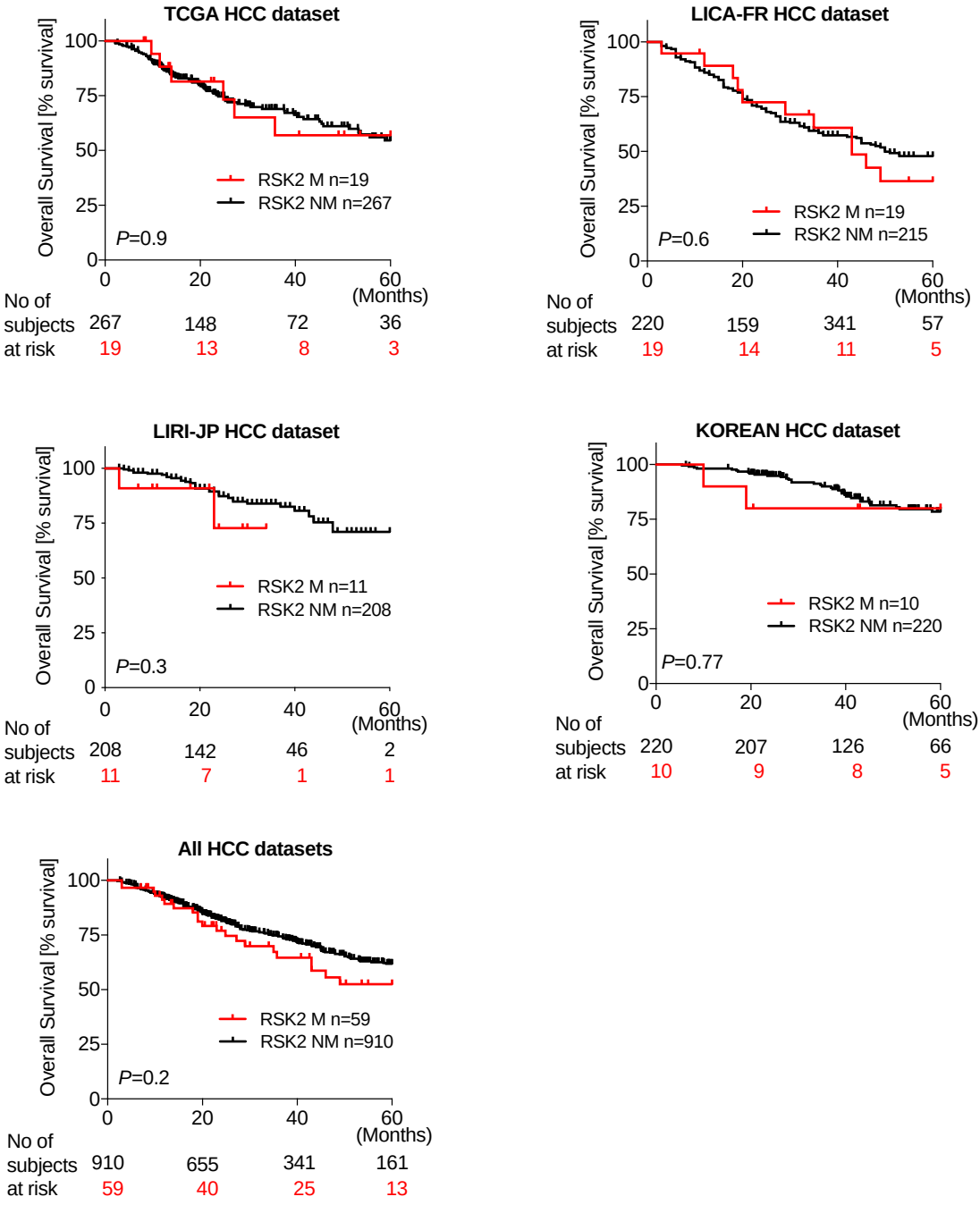

Fig. S2. Prognosis of HCC patients from four independent datasets depending on RSK2 mutational status. Kaplan-Meier curves for overall survival in patients with R0 resected HCCs stratified according to RSK2 mutation status. Log-rank test was used to statistically compare survival curves.

A

Mouse model	Transgenic (9 months)					DEN + PB (9 months)		
Oncogenic cooperation tested	*Rsk2*^{wt} ; *Axin1*^{wt}/AhCre	***Rsk2***$^{-/y}$; *Axin1*^{wt}/AhCre	*Rsk2*^{wt} ; *Axin1*$^{fl/fl}$/AhCre	***Rsk2***$^{-/y}$; *Axin1*$^{fl/fl}$/AhCre	*P*-value	*Rsk2*^{wt} ; *Ctnnb1*	*Rsk2*$^{-/y}$; *Ctnnb1*	*P*-value
# of mice	n=9	n=8	n=10	n=9		n=10	n=8	
Tumor frequency	0%	0%	20%	11.1%	0.33	20%	87.5%	**0.015**
# of nodules/mouse mean ± SD	0	0	4.5 ± 4.9	2	n.d	1.5 ± 0.7	1.9 ± 1.5	1
Total # of nodules analyzed in IHC	0	0	9	2		3	13	
GS + nodules	-	-	11.1%	50%	0.34	66.7%	46.1%	1
Nuclear ß-catenin + nodules	-	-	0%	0%	1	0%	38.5%	0.52
P-ERK + nodules	-	-	11.1%	100%	0.054	33%	25%	1
P-ERK H-score/ nodule mean ± SD	-	-	3.3 ± 10	55 ± 35.4	**0.036**	1.7 ± 2.9	11.7 ± 34.3	1
Liver/body weight % mean ± SD	4.2 ± 0.5	4.3 ± 0.4	5.6 ± 0.7	5.9 ± 1.4	**<0.0001**	5.7 ± 0.6	5.9 ± 0.54	0.53
Cellular atypia (NTL)	22.2%	0%	70%	55.5%	**0.01**	90%	62.5%	1

B

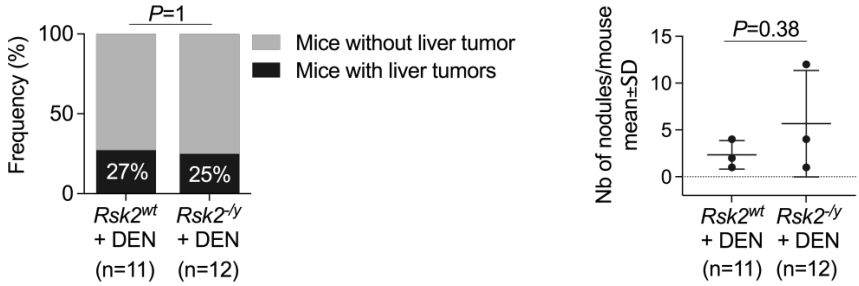

C

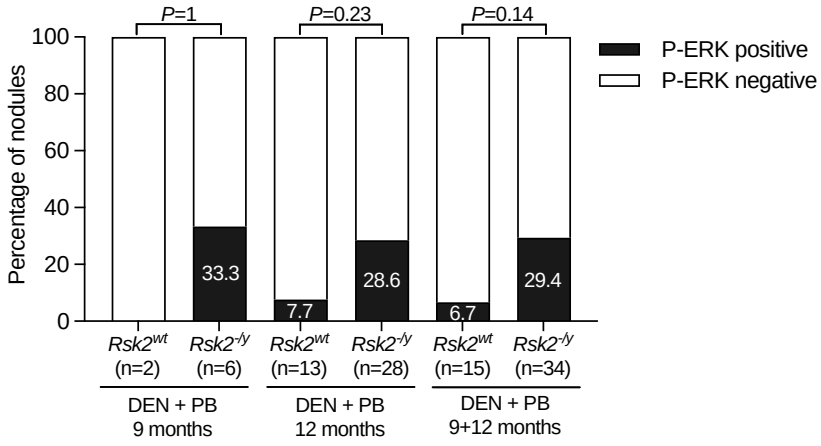

	DEN + PB (9 months)		DEN + PB (12 months)		DEN + PB (9+12 months)	
	Rsk2^{wt}	*Rsk2*$^{-/y}$	*Rsk2*^{wt}	*Rsk2*$^{-/y}$	*Rsk2*^{wt}	*Rsk2*$^{-/y}$
Number of nodules analyzed	2	6	13	28	15	34
P-ERK **H-score**/nodule Mean	0	21.7	0.77	4.3	0.67	7.3
P-ERK **H-score**/nodule SD	0	48.3	2.8	10.9	2.6	22.3
P-value	0.79		0.20		0.11	

Fig. S3. Tumor appearance and histological features in two mouse models combining Rsk2 null or wild-type allele to another oncogenic event. (A) Table comparing liver tumor appearance and their immunohistochemical features, and histological features of the non-tumor liver (NTL) in 9 months-old mice from different genotypes and mouse models combining RSK2 inactivation with AXIN1 inactivation (transgenic model) or ß-catenin

activation (DEN+PB model) (Chi-square test and Fisher's exact test were used for categorial variables or Mann-Whitney test for continuous variables). Of note, the two nodules positive for phospho-ERK in mice inactivated for both RSK2 and AXIN1 also display an activating mutation in HRAS at codon 61. (B) Comparison of liver tumor incidence and number in RSK2 inactivated (*Rsk2*$^{-/y}$) and wild-type (*Rsk2*^{wt}) mice treated with DEN at 6 weeks of age. Statistical significance between groups was assessed using a Fisher's exact test for tumor incidence and a two-tailed t-test for tumor number. (C) Analysis of phospho-ERK immunostaining in the DEN/PB mouse model by restricting the analysis only to GS and/or nuclear ß-catenin positive tumors showing no significant difference between RSK2 inactivated and wild-type mice (Fisher's exact test and Mann-Whitney test). DEN: diethylnitrosamine; PB: phenobarbital

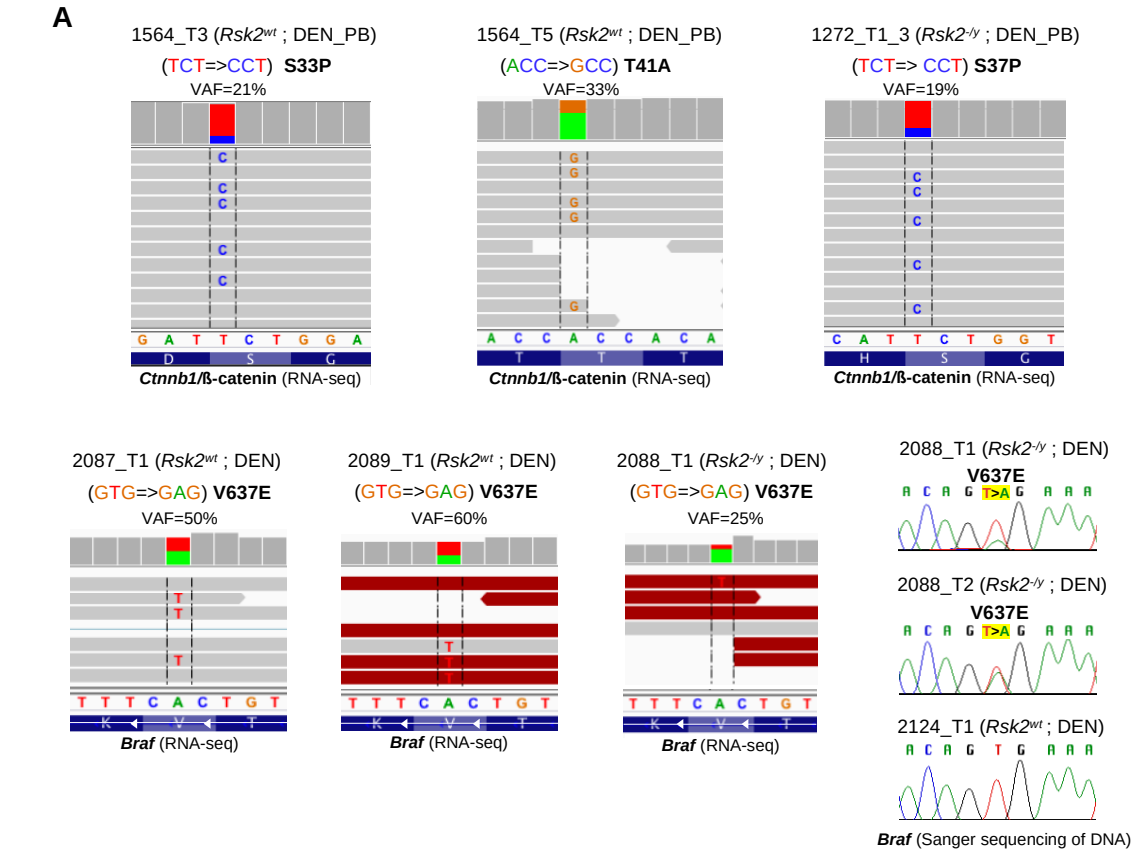

Fig. S4. Oncogenic mutations identified in HCC developed in the three different mouse models. (A) Upper panel: ß-catenin activating mutations identified by RNA-sequencing in three independent HCCs developed in two mice with *Rsk2* null (*Rsk2*$^{-/y}$, n=1) or wild-type

(*Rsk2*^{wt}, n=2) allele treated with DEN and PB. Bottom panel: *Braf* activating mutations identified by RNA-sequencing (reverse complement sequence) and Sanger sequencing of DNA (forward sequence) in 4/5 independent HCCs developed in four mice with *Rsk2* null (n=2) or wild-type allele (n=3). (B) *Hras* activating mutations identified by RNA-sequencing in three independent HCCs from two mice with double inactivation of RSK2 and AXIN1 (*Rsk2*$^{-/y}$; *Axin1*$^{fl/fl}$/Cre). DEN: diethylnitrosamine ; PB: phenobarbital ; VAF: variant allele frequency.

A

Canonical positive ß-catenin target genes

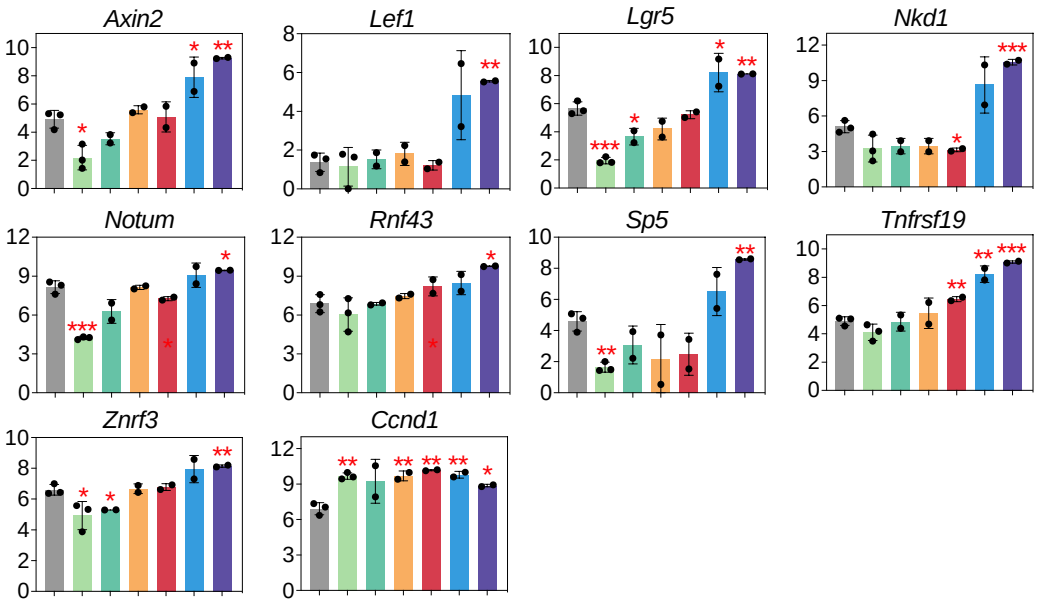

Liver specific ß-catenin positive and negative target genes

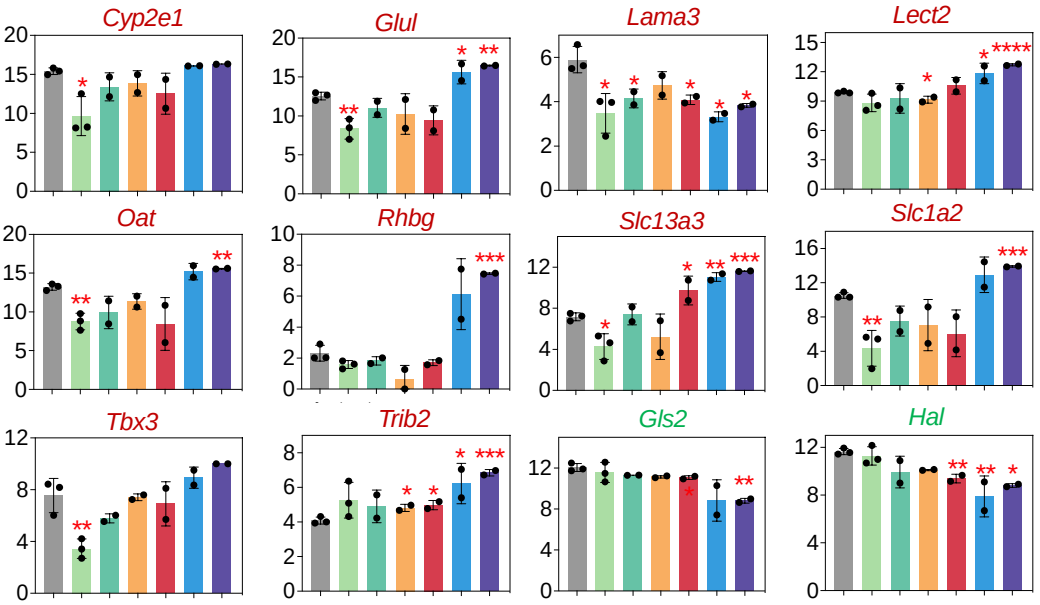

Mean expression of positive ß-catenin target genes

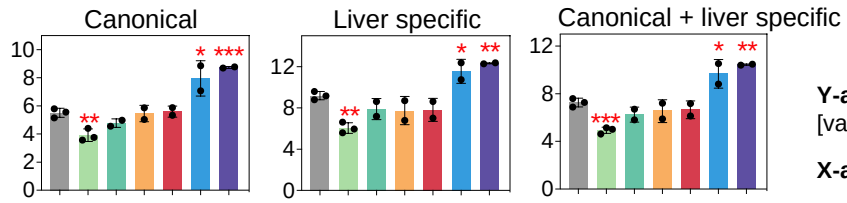

Y-axis: mRNA level (RNA-seq)
[variance stabilized values: mean +/- SD]

X-axis: mouse model

Normal liver:
Rsk2^{wt} ; *Axin1*^{wt}/AhCre (10.5 months)

Liver tumors:
Rsk2^{wt} ; DEN
Rsk2$^{-/y}$; DEN
Rsk2^{wt} ; *Axin1*$^{fl/fl}$/AhCre
Rsk2$^{-/y}$; *Axin1*$^{fl/fl}$/AhCre
Rsk2^{wt} ; DEN_PB (ß-catenin mutated)
Rsk2$^{-/y}$; DEN_PB (ß-catenin mutated)

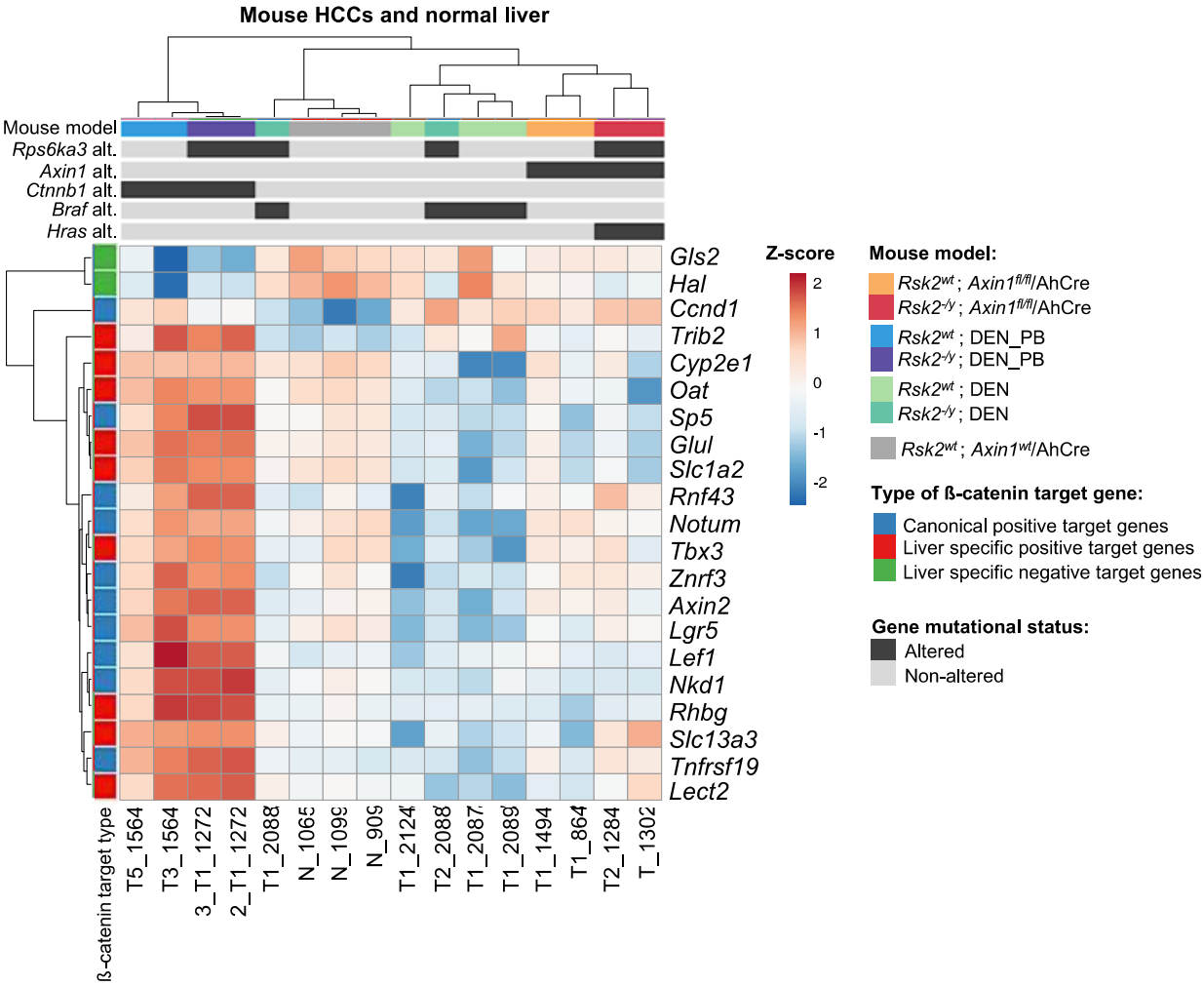
Mouse HCCs and normal liver
Mouse model
Rps6ka3 alt.
Axin1 alt.
Ctnnb1 alt.
Braf alt.
Hras alt.
Gls2
Hal
Ccnd1
Trib2
Cyp2e1
Oat
Sp5
Glul
Slc1a2
Rnf43
Notum
Tbx3
Znrf3
Axin2
Lgr5
Lef1
Nkd1
Rhbg
Slc13a3
Tnfrsf19
Lect2
ß-catenin target type
T5_1564
T3_1564
3_T1_1272
2_T1_1272
T1_2088
N_1065
N_1099
N_905
T1_2124
T2_2088
T1_2087
T1_2089
T1_1494
T1_864
T2_1284
T_1302
Z-score
2
1
0
-1
-2
Mouse model:
Rsk2wt ; Axin1fl/fl/AhCre
Rsk2-/y ; Axin1fl/fl/AhCre
Rsk2wt ; DEN_PB
Rsk2-/y ; DEN_PB
Rsk2wt ; DEN
Rsk2-/y ; DEN
Rsk2wt ; Axin1wt/AhCre
Type of ß-catenin target gene:
Canonical positive target genes
Liver specific positive target genes
Liver specific negative target genes
Gene mutational status:
Altered
Non-altered

B **Canonical positive ß-catenin target genes**

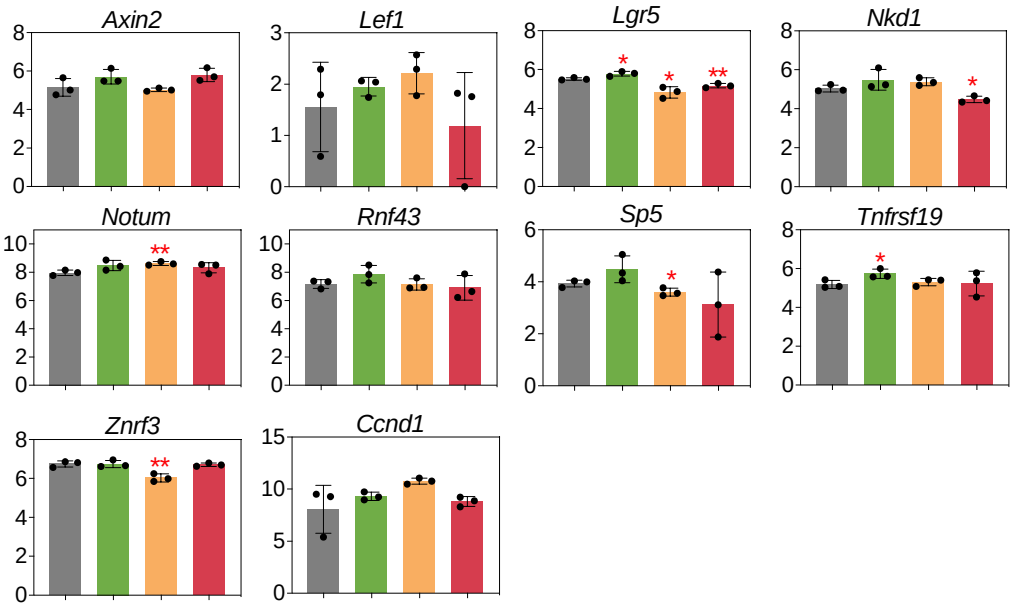

Liver specific ß-catenin positive and negative target genes

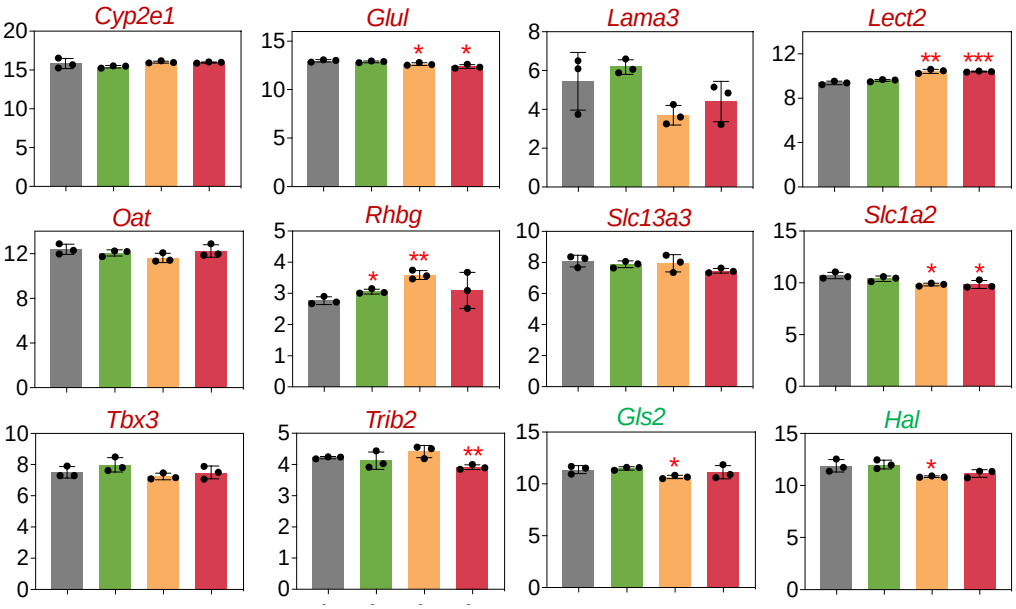

Mean expression of positive ß-catenin target genes

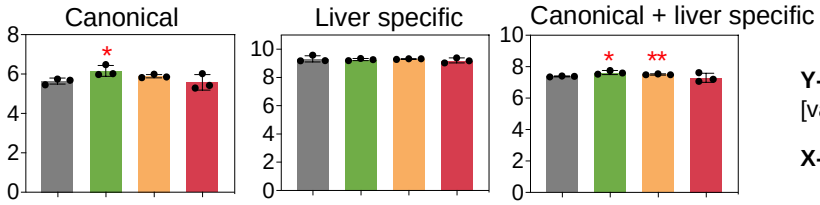

Y-axis: mRNA level (RNA-seq)
[variance stabilized values: mean +/- SD]

X-axis: mouse model

Mouse normal liver (6 weeks):

Rsk2^{wt} ; *Axin1*^{wt}/AhCre
Rsk2$^{-/y}$; *Axin1*^{wt}/AhCre
Rsk2^{wt} ; *Axin1*$^{fl/fl}$/AhCre
Rsk2$^{-/y}$; *Axin1*$^{fl/fl}$/AhCre

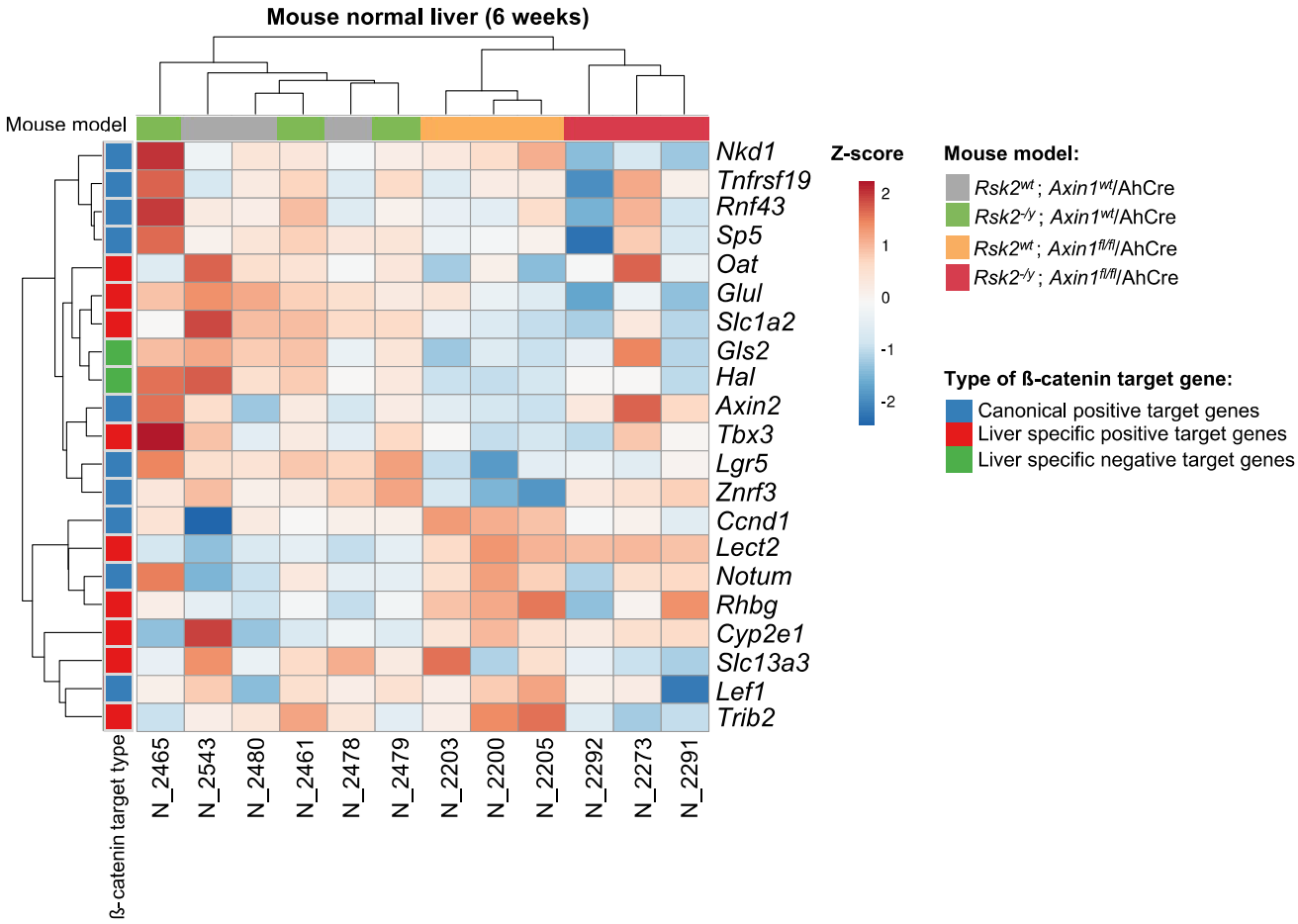

Fig. S5. Analysis of ß-catenin target genes expression in mouse liver tumors and in normal liver. (A) Bar plots and hierarchical clustering showing transcriptional deregulation of canonical and liver specific ß-catenin target genes only in liver tumors from the DEN/PB mouse model harboring ß-catenin activating mutations, compared to non-tumor liver tissues (two-tailed t-test). (B) Bar plots and hierarchical clustering showing no obvious transcriptional deregulation of ß-catenin target genes in non-tumor liver tissues in AXIN1 inactivated mice regardless of *Rsk2* genotype compared to wild-type mice at 6 weeks of age (two-tailed t-test). ß-catenin target genes described in humans were taken from a previous report by Abitbol *et al.* [25] (except for *Ccnd1)*. *Lama3* was excluded from the calculation of the mean liver specific target genes and from hierarchical clustering analyses as in mouse, it does not behave as a ß-catenin positive target.

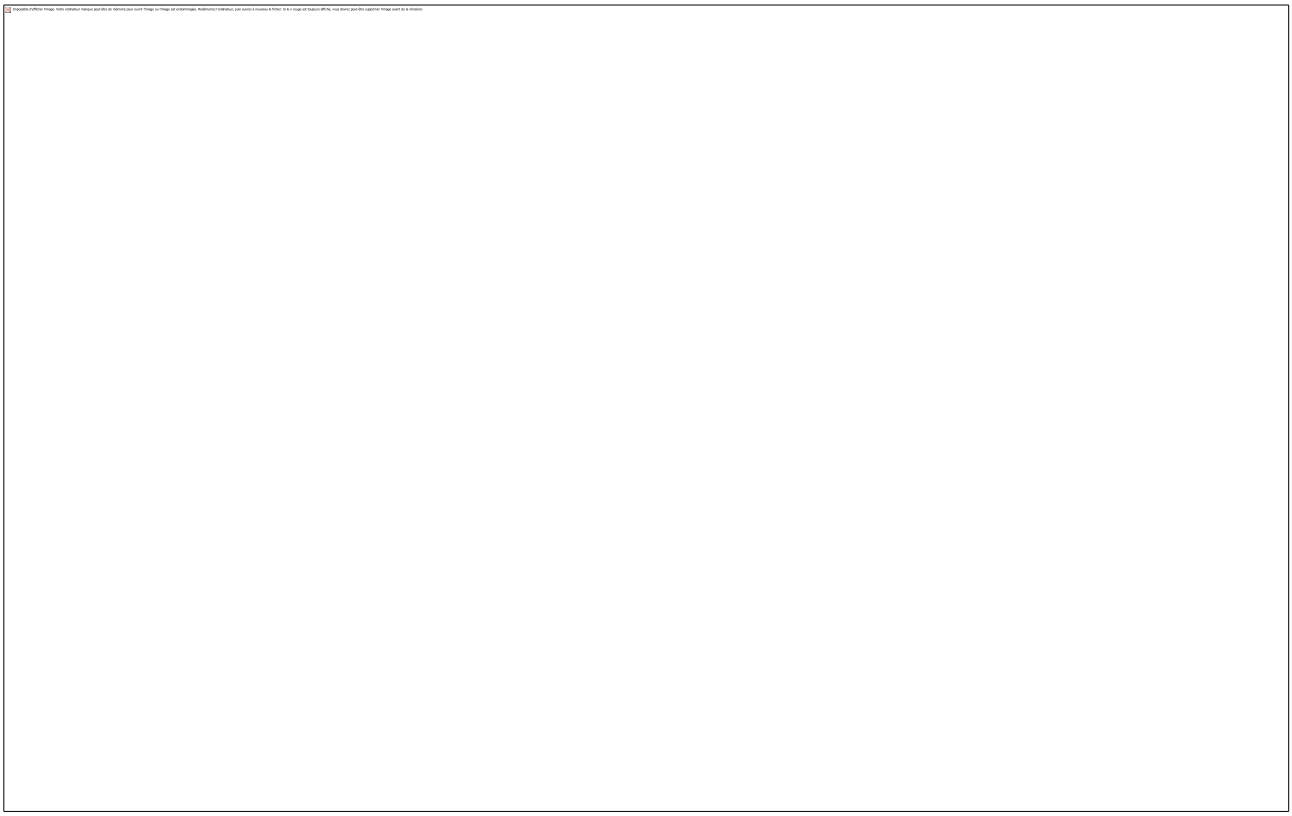

Fig. S6. Immunohistological features of the 1284_T1 tumor developed in a mouse with double inactivation of RSK2 and AXIN1. HES staining and immunostaining of glutamine-synthetase (GS) and ß-catenin showing tumor heterogeneity with a map-like GS pattern usually typically found in focal nodular hyperplasia [26].

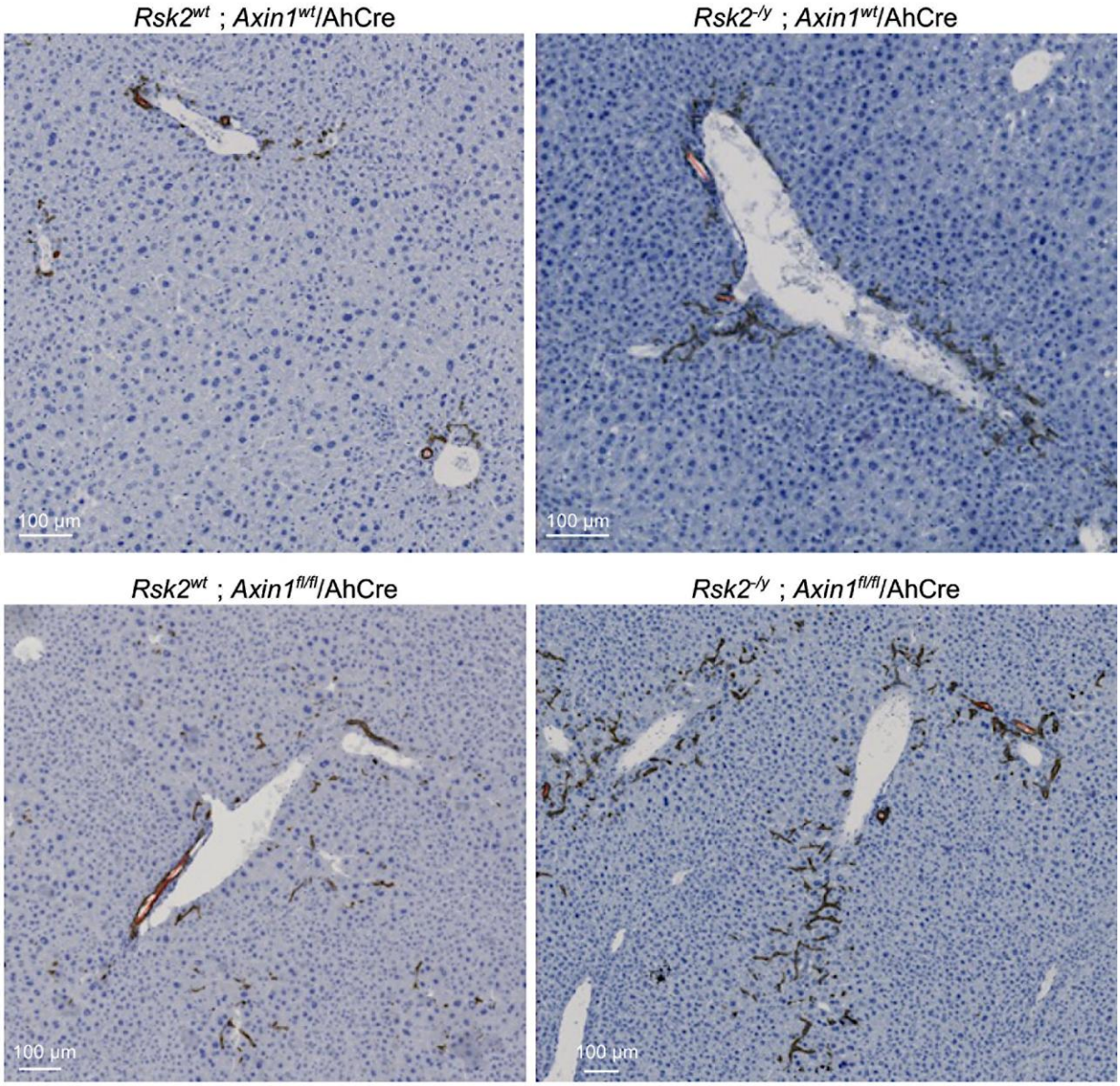

Fig. S7. Increase number of oval cells in RSK2 inactivated livers. Representative pictures showing single, cluster or cords of oval cells mainly in the peri-portal region in 6-weeks old mice liver from mice inactivated for RSK2 (*Rsk2*$^{-/y}$; *Axin1*^{wt}/AhCre), AXIN1 (*Rsk2*^{wt} ; *Axin1*$^{fl/fl}$/AhCre) or both RSK2 and AXIN1 (*Rsk2*$^{-/y}$; *Axin1*$^{fl/fl}$/AhCre) compared to wild-type mice (*Rsk2*^{wt} ; *Axin1*^{wt}/AhCre). Interlobular bile ducts (marked by red mark) were excluded from the analysis.

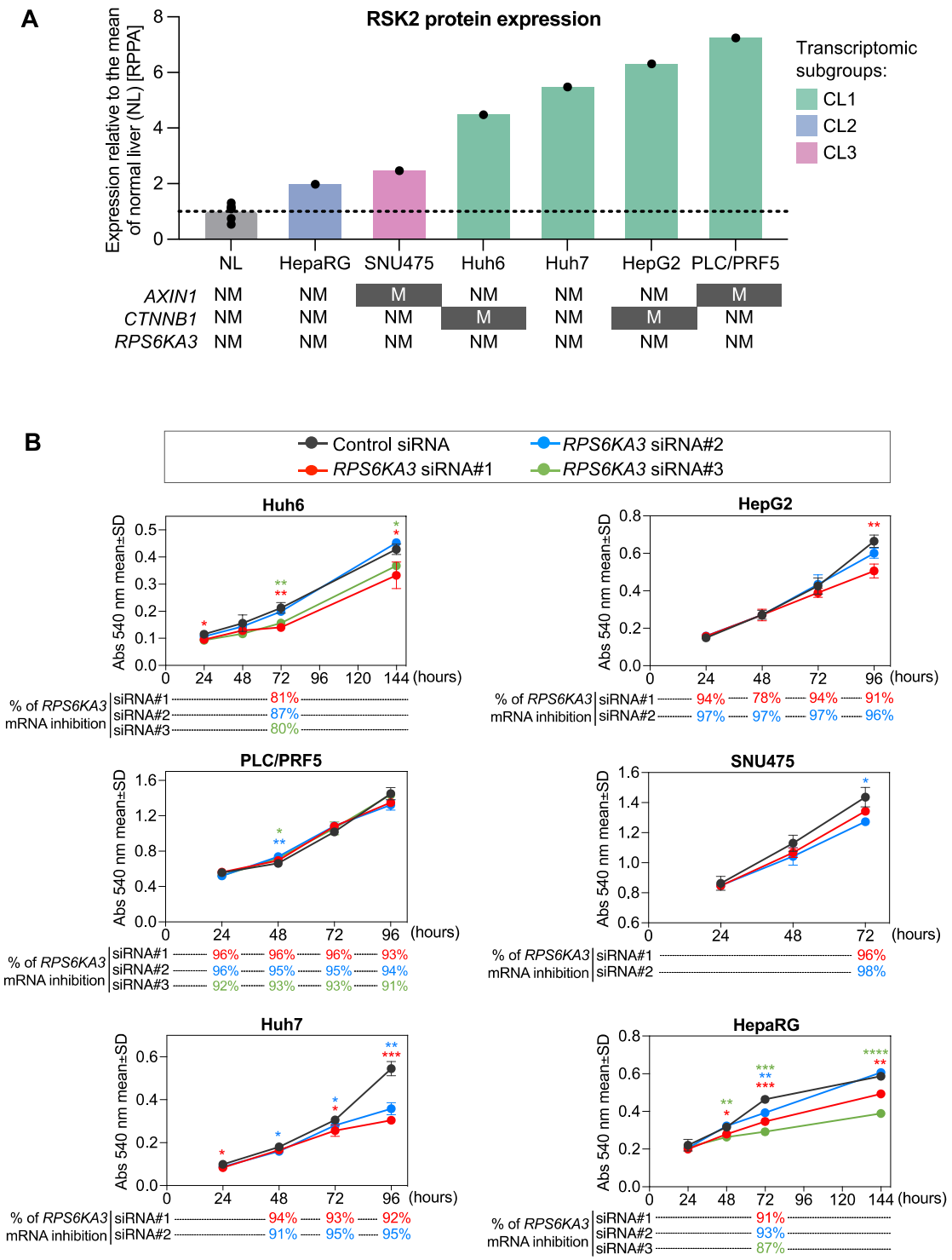
A
RSK2 protein expression
Expression relative to the mean of normal liver (NL) [RPPA]
Transcriptomic subgroups:
CL1
CL2
CL3
NL
HepaRG
SNU475
Huh6
Huh7
HepG2
PLC/PRF5
AXIN1 NM NM M NM NM NM M
CTNNB1 NM NM NM M NM M NM
RPS6KA3 NM NM NM NM NM NM NM
B
Control siRNA
RPS6KA3 siRNA#1
RPS6KA3 siRNA#2
RPS6KA3 siRNA#3
Huh6
Abs 540 nm mean±SD
(hours)
% of RPS6KA3 mRNA inhibition
siRNA#1 81%
siRNA#2 87%
siRNA#3 80%
HepG2
siRNA#1 94% 78% 94% 91%
siRNA#2 97% 97% 97% 96%
PLC/PRF5
siRNA#1 96% 96% 96% 93%
siRNA#2 96% 95% 95% 94%
siRNA#3 92% 93% 93% 91%
SNU475
siRNA#1 96%
siRNA#2 98%
Huh7
siRNA#1 94% 93% 92%
siRNA#2 91% 95% 95%
HepaRG
siRNA#1 91%
siRNA#2 93%
siRNA#3 87%

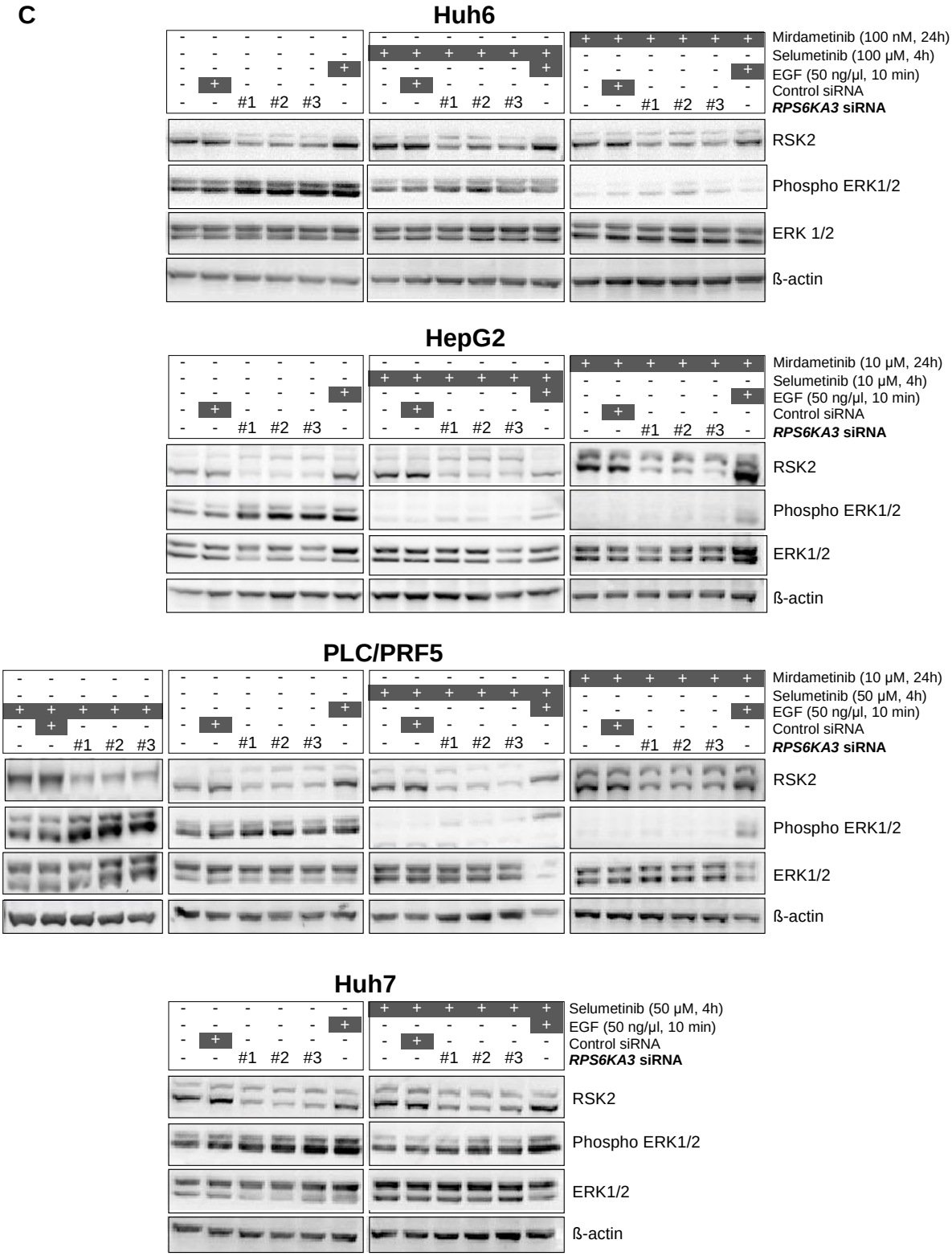

Fig. S8. RSK2 knockdown in various oncogenic contexts does not promote cell survival in human liver cancer cell lines but increases phospho-ERK levels that can be effectively inhibited by MEK inhibitors. (A) RSK2 protein level analyzed by RPPA in 6 human liver cancer cell lines (data previously published [14]) relative to the mean expression

in 6 human normal livers represented by the horizontal dashed line. The mutational status of *AXIN1*, *CTNNB1* and *RPS6KA3* genes is indicated below for each cell line as follows: NM, non-mutated; M, mutated. Transcriptomic classification of cell lines was previously defined as follows from the most to the less differentiated subgroups: CL1: hepatoblast-like, CL2 mixed epithelial-mesenchymal and CL3: mesenchymal-like [14]. (B) Cell survival assessed by MTT assay in 6 human liver cancer cell lines transfected with three different *RPS6KA3* siRNAs or with a control siRNA showing no increase following RSK2 knockdown neither in the 4 cell lines mutated for *AXIN1* (n=2) or *CTNNB*1 (n=2) recapitulating the most frequent co-occurring events with RSK2 loss, nor in the 2 cell lines non-mutated for these two genes. Silencing efficacy of *RPS6KA3* mRNA was assessed for each siRNA by qRT-PCR and is expressed as percentage of inhibition relative to the control siRNA for the corresponding times analyzed. * $P<0.05$, ** $P<0.01$, *** $P<0.001$, **** $P<0.0001$ indicate significant difference compared to the control siRNA (two tailed t-test). (C) Western-blot analysis of 4 liver cancer cell lines showing an increase in ERK phosphorylation following RSK2 silencing (data previously published [1]) compared to cells transfected with reagent alone or non-specific control siRNA with efficient inhibition after treatment with two MEK inhibitors (selumetinib and mirdametinib).
EGF stimulation in serum-free medium was performed as a positive control for ERK1/2 phosphorylation or to uncover the impact of RSK2 inhibition on ERK signaling. ß-actin was used as a loading control.

Supplementary tables (see excel file)

Table S1. Comparison of clinical features between patients with RSK2-mutated HCCs and patients with RSK2-non-mutated HCCs.

Table S2. HCCs analyzed by RNA sequencing in the different mouse models combining Rsk2 null (*Rsk2*$^{-/y}$) or wild-type (*Rsk2*^{wt}) allele with another oncogenic event.

Table S3. List of the 372-gene expression signature (one-to-one orthologous genes) used for the transcriptomic comparison of mouse and human HCCs.

Table S4. List of genes differentially expressed in mice liver inactivated for RSK2 and/or AXIN1 at 6 weeks of age.

Table S5. Gene set enrichment analysis in mice liver inactivated for RSK2 and/or AXIN1 at 6 weeks of age.

Supplementary references

Author names in bold designate shared co-first authorship

[1] **Schulze K, Imbeaud S, Letouzé E**, Alexandrov LB, Calderaro J, Rebouissou S, et al. Exome sequencing of hepatocellular carcinomas identifies new mutational signatures and potential therapeutic targets. Nat Genet 2015;47:505–11. https://doi.org/10.1038/ng.3252.

[2] **Letouzé E, Shinde J,** Renault V, Couchy G, Blanc J-F, Tubacher E, et al. Mutational signatures reveal the dynamic interplay of risk factors and cellular processes during liver tumorigenesis. Nat Commun 2017;8:1315. https://doi.org/10.1038/s41467-017-01358-x.

[3] Bayard Q, Meunier L, Peneau C, Renault V, Shinde J, Nault J-C, et al. Cyclin A2/E1 activation defines a hepatocellular carcinoma subclass with a rearrangement signature of replication stress. Nat Commun 2018;9:5235. https://doi.org/10.1038/s41467-018-07552-9.

[4] **Hirsch TZ, Negulescu A**, Gupta B, Caruso S, Noblet B, Couchy G, et al. BAP1 mutations define a homogeneous subgroup of hepatocellular carcinoma with fibrolamellar-like features and activated PKA. J Hepatol 2020;72:924–36. https://doi.org/10.1016/j.jhep.2019.12.006.

[5] Nault J-C, Martin Y, Caruso S, Hirsch TZ, Bayard Q, Calderaro J, et al. Clinical Impact of Genomic Diversity From Early to Advanced Hepatocellular Carcinoma. Hepatology 2020;71:164–82. https://doi.org/10.1002/hep.30811.

[6] Cancer Genome Atlas Research Network. Electronic address: wheeler@bcm.edu, Cancer Genome Atlas Research Network. Comprehensive and Integrative Genomic Characterization of Hepatocellular Carcinoma. Cell 2017;169:1327-1341.e23. https://doi.org/10.1016/j.cell.2017.05.046.

[7] Ahn S-M, Jang SJ, Shim JH, Kim D, Hong S-M, Sung CO, et al. Genomic portrait of resectable hepatocellular carcinomas: implications of RB1 and FGF19 aberrations for patient stratification. Hepatology 2014;60:1972–82. https://doi.org/10.1002/hep.27198.

[8] Fujimoto A, Furuta M, Totoki Y, Tsunoda T, Kato M, Shiraishi Y, et al. Whole-genome mutational landscape and characterization of noncoding and structural mutations in liver cancer. Nat Genet 2016;48:500–9. https://doi.org/10.1038/ng.3547.

[9] Bayard Q, Caruso S, Couchy G, Rebouissou S, Bioulac Sage P, Balabaud C, et al. Recurrent chromosomal rearrangements of ROS1, FRK and IL6 activating JAK/STAT pathway in inflammatory hepatocellular adenomas. Gut 2020;69:1667–76. https://doi.org/10.1136/gutjnl-2019-319790.

[10] Delaunoy J, Abidi F, Zeniou M, Jacquot S, Merienne K, Pannetier S, et al. Mutations in the X-linked RSK2 gene (RPS6KA3) in patients with Coffin-Lowry syndrome. Hum Mutat 2001;17:103–16. https://doi.org/10.1002/1098-1004(200102)17:2<103::AID-HUMU2>3.0.CO;2-N.

[11] Delaunoy JP, Dubos A, Marques Pereira P, Hanauer A. Identification of novel mutations in the RSK2 gene (RPS6KA3) in patients with Coffin-Lowry syndrome. Clin Genet 2006;70:161–6. https://doi.org/10.1111/j.1399-0004.2006.00660.x.

[12] Gao J, Aksoy BA, Dogrusoz U, Dresdner G, Gross B, Sumer SO, et al. Integrative analysis of complex cancer genomics and clinical profiles using the cBioPortal. Sci Signal 2013;6:pl1. https://doi.org/10.1126/scisignal.2004088.

[13] Cerami E, Gao J, Dogrusoz U, Gross BE, Sumer SO, Aksoy BA, et al. The cBio cancer genomics portal: an open platform for exploring multidimensional cancer genomics data. Cancer Discov 2012;2:401–4. https://doi.org/10.1158/2159-8290.CD-12-0095.

[14] **Caruso S, Calatayud A-L, Pilet J**, La Bella T, Rekik S, Imbeaud S, et al. Analysis of Liver Cancer Cell Lines Identifies Agents With Likely Efficacy Against Hepatocellular Carcinoma and Markers of Response. Gastroenterology 2019;157:760–76. https://doi.org/10.1053/j.gastro.2019.05.001.

[15] Yang X, Matsuda K, Bialek P, Jacquot S, Masuoka HC, Schinke T, et al. ATF4 is a substrate of RSK2 and an essential regulator of osteoblast biology; implication for Coffin-Lowry Syndrome. Cell 2004;117:387–98. https://doi.org/10.1016/s0092-8674(04)00344-7.

[16] Feng GJ, Cotta W, Wei XQ, Poetz O, Evans R, Jardé T, et al. Conditional disruption of Axin1 leads to development of liver tumors in mice. Gastroenterology 2012;143:1650–9. https://doi.org/10.1053/j.gastro.2012.08.047.
[17] Ireland H, Kemp R, Houghton C, Howard L, Clarke AR, Sansom OJ, et al. Inducible Cre-mediated control of gene expression in the murine gastrointestinal tract: effect of loss of beta-catenin. Gastroenterology 2004;126:1236–46. https://doi.org/10.1053/j.gastro.2004.03.020.
[18] Lu W-Y, Bird TG, Boulter L, Tsuchiya A, Cole AM, Hay T, et al. Hepatic progenitor cells of biliary origin with liver repopulation capacity. Nat Cell Biol 2015;17:971–83. https://doi.org/10.1038/ncb3203.
[19] Roskams T, Yang SQ, Koteish A, Durnez A, DeVos R, Huang X, et al. Oxidative stress and oval cell accumulation in mice and humans with alcoholic and nonalcoholic fatty liver disease. Am J Pathol 2003;163:1301–11. https://doi.org/10.1016/S0002-9440(10)63489-X.
[20] Abou Monsef Y, Kutsal O. Immunohistochemical evaluation of hepatic progenitor cells in different types of feline liver diseases. J Vet Med Sci 2021;83:613–21. https://doi.org/10.1292/jvms.20-0435.
[21] Bankhead P, Loughrey MB, Fernández JA, Dombrowski Y, McArt DG, Dunne PD, et al. QuPath: Open source software for digital pathology image analysis. Sci Rep 2017;7:16878. https://doi.org/10.1038/s41598-017-17204-5.
[22] Buchmann A, Karcier Z, Schmid B, Strathmann J, Schwarz M. Differential selection for B-raf and Ha-ras mutated liver tumors in mice with high and low susceptibility to hepatocarcinogenesis. Mutat Res 2008;638:66–74. https://doi.org/10.1016/j.mrfmmm.2007.08.015.
[23] Boyault S, Rickman DS, de Reyniès A, Balabaud C, Rebouissou S, Jeannot E, et al. Transcriptome classification of HCC is related to gene alterations and to new therapeutic targets. Hepatology 2007;45:42–52. https://doi.org/10.1002/hep.21467.
[24] Metsalu T, Vilo J. ClustVis: a web tool for visualizing clustering of multivariate data using Principal Component Analysis and heatmap. Nucleic Acids Res 2015;43:W566-570. https://doi.org/10.1093/nar/gkv468.
[25] **Abitbol S, Dahmani R**, Coulouarn C, Ragazzon B, Mlecnik B, Senni N, et al. AXIN deficiency in human and mouse hepatocytes induces hepatocellular carcinoma in the absence of β-catenin activation. J Hepatol 2018;68:1203–13. https://doi.org/10.1016/j.jhep.2017.12.018.
[26] Rebouissou S, Couchy G, Libbrecht L, Balabaud C, Imbeaud S, Auffray C, et al. The beta-catenin pathway is activated in focal nodular hyperplasia but not in cirrhotic FNH-like nodules. J Hepatol 2008;49:61–71. https://doi.org/10.1016/j.jhep.2008.03.013.